Magnetically modified double slit based x-ray interferometry

S. Atkar,[1] Z. Tumbleson,[2,3] S. A. Morley,[4] N. Burdet,[5] A. Islegen-Wojdyla,[4] K. A. Goldberg,[4] A. Scholl,[4] S. A. Montoya,[6] Trinanjan Datta,[7] and S. Roy[4,3,*]

[1] *Department of Physics, Indian Institute of Technology, Guwahati, Assam 781039, India*
[2] *Materials Sciences Division, Lawrence Berkeley National Laboratory, Berkeley, California 94720, USA*
[3] *Department of Physics, University of California, Santa Cruz, California 95064, USA*
[4] *Advanced Light Source, Lawrence Berkeley National Laboratory, Berkeley, California 94720, USA*
[5] *Linac Coherent Light Source, SLAC National Accelerator Laboratory, Menlo Park, California 94720*
[6] *Center for Magnetic Recording Research, University of California San Diego, La Jolla, California, USA*
[7] *Department of Physics and Biophysics, Augusta University, Augusta, Georgia 30912, USA*

We demonstrate an experimental approach to determine magneto-optical effects which combines x-ray magnetic circular dichroism (XMCD) with x-ray interferometry, based on the concepts of Young's canonical double slit. By covering one of two slits with a magnetic thin film and employing XMCD, we show that it is possible to determine both the real and the imaginary parts of the complex refractive index by measuring the fringe shifts that occur due to a change in the sample magnetization. Our hybrid spectroscopic-interferometric methodology provides a means to probe changes in the magnetic refractive index in terms of the electron spin moment.

Fundamental understanding of x-ray-matter interaction is the key to several advanced characterization methods with wide applications in many scientific areas [1–5]. The development of these methods relies on accurate and quantitative measurements of optical parameters [6–8]. Depending on the photon energy, x-rays can be used to extract different properties of a material or a sample. Soft x-rays (100-2000 eV), in particular, are used as a spectroscopic probe as it covers binding energies of several important elements such as carbon, oxygen, nitrogen. In addition, by tuning the incident x-ray beam energy to a L or M edge of a transition metal or rare earth element (the resonant condition) where the spectroscopic response is maximal, it is possible to achieve enhanced sensitivity to orbital and spin properties [9, 10]. An important example of a resonance based spectroscopy technique is x-ray magnetic circular dichroism (XMCD), which is the differential absorption of x-rays with opposite helicities [11, 12]. Together with x-ray absorption spectroscopy (XAS) and XMCD, it is possible to determine the complex refractive index $n(\omega) = 1 - \delta(\omega) + i\beta(\omega)$, where δ and β are the real and imaginary components, respectively, describe the dispersive and the absorptive aspects of the x-ray-photon-material interaction. While experimental techniques have measured δ and β, these approaches were focused towards phase retrieval for imaging purposes [13–16]. For spectroscopic and metrology applications one can envision combining XMCD with double slit diffraction. XMCD provides element-specific information about the magnetic moment, and can be utilized to obtain element-specific spin and orbital magnetic moments of the electron [2, 11, 17], while the double slit fringe pattern shifts can be used as a metric to find changes in the refractive index.

In this Letter, we propose an innovative experimental set-up that integrates interferometry and XMCD to determine the magnetic refractive index. Utilizing a modified Young's double-slit arrangement (see Fig. 1a), we determine interference fringe pattern shifts induced by changes in the magnetic part of the refractive index of an Fe/Gd thin film heterostructure under an applied external magnetic field [18]. We fabricated a specialized double slit with one open slit, and the other covered by the heterostructure film. The slits were illuminated by a coherent x-ray beam tuned to the resonant L_3 edge of Fe (707 eV). Light passing through the slits produces an interference fringe pattern on an x-ray charge-coupled device (CCD) camera downstream.

The spin-dependent interaction of circularly polarized x-rays induce magnetic sensitivity in the double-slit diffraction pattern. In our measurements, we track the lateral shift of the fringe pattern for both the circularly *plus* (σ_+) and the *minus* (σ_-) polarized x-rays. By applying a varying external magnetic field and tracing hysteresis loops in the resultant pattern shift, we observe the coupling of optical properties to the applied field. This combination of interferometry with XMCD provides sensitivity to magnetization changes and enables us to identify the difference in the population of spin-up and spin-down electrons that gives rise to a net moment in the material.

At the resonant condition, the scattering factors become a complex quantity. The contribution to the scattering signal from the charge and magnetism can be de-

* sroy@lbl.gov

termined. Consequently, it is possible to determine the charge and magnetic contribution to dispersion δ and β, as well as charge and magnetic thicknesses [19, 20]. The interferometric method allows us to retrieve $\delta(\omega)$. Upon transmission, the phase (or *optical path length*) of the light passing through the covered slit varies relative to the open slit. The optical path difference Δl is related to the measured phase by $\phi = k\Delta l$, where λ is the x-ray wavelength and $k = 2\pi/\lambda$ is the wavenumber. For a material thickness t_f, the path difference induced by transmission is related to the real-part of the refractive index by $(n(\omega) - 1)t_f = -\delta(\omega)t_f$. With prior knowledge of $\delta(\omega)$ (or thickness) and by analyzing the fringes of the resulting intensity interferogram as a function of the applied magnetic field, we can determine the *magnetic* thickness, i.e., the thickness of the sample that produces magnetism and may or may not be equal to the actual thickness of the film of the sample (or *magnetic* dispersion ($\delta(\omega)_{magnetic}$)).

Experiments were conducted at the COSMIC-Scattering beamline (BL 7.0.1.1) of the Advanced Light Source at Lawrence Berkeley National Laboratory, using a canonical Young's Double Slit configuration. (See Fig. 1(a).) A high degree of transverse coherence in the incident x-ray beam was established with a 7 µm pinhole placed about 5 mm before the slits. The energy of the incident beam was varied across the Fe L edges (700-730 eV) and data was measured using circularly polarized light. Within this energy range variations in the coherent flux, degree of polarization of the incident beam were negligible. The double slit consists of two slits, each nominally 100 nm wide, separated by ≈ 10 µm, center to center. The 100 nm $\times$ 60 µm slits were created by focused ion beam milling, producing one through-slit and one with the sample. The slit covered with our sample, consisted of a 34 nm-thick Fe/Gd multilayer. A 600-nm-thick layer of Au was deposited on its back-side to provide the slit mask with transmittance below 10^{-4}. The Fe/Gd specimen was sputter deposited at room temperature in an ultrahigh vacuum environment under 3 mm-Torr of Argon. To grow the multilayer, alternating Fe 0.34 nm and Gd 0.40 nm films were deposited, and the process was repeated until a 100 bilayer repetitions were achieved. A 5 nm thick seed and capping layer of Ta was used to protect the sample from oxidation. The sample was grown on an SiN membrane that is 100 nm thick on a 5 mm $\times$ 5 mm Si frame. Details of the Fe/Gd sample synthesis and characterization have been published elsewhere (see references [21]). A Charge Coupled Device (CCD) camera, used to record the interference patterns, was placed 93 cm downstream of the slits. Images were acquired with 400 ms exposure time, a frame size of 1024 $\times$ 1024 pixels, with $s_{\text{pixel}} = 13.5$ µm square pixels. In the data collection, 20 successive frames were averaged. A central beam-stop blocked the bright central region to prevent detector saturation and increase the dynamic range of the fringe pattern measurement. The incident beam energy was tuned to the Fe L_3 edge to achieve the resonant condition so as to get the magnetic sensitivity in the data.

Two types of measurements were performed: (a) diffraction measurements as a function of incident beam energies, and (b) measurement as a function of the applied magnetic field. For the magnetic field experiments, and an out-of-plane external magnetic field was applied *in-situ* within the field range of -1500 G to +1500 G, and back. We note that although the saturation magnetization is reported to be $\sim$ 5000 G, the experimental end-station allowed us to investigate only up to 1500 G. All the measurements were performed using σ_+ and σ_- incident x-ray light tuned to the Fe L_3 edge.

We extracted the fringe-pattern shifts (ΔY) from the recorded x-ray intensity images of the diffraction-interference pattern via a phase-correlation image registration algorithm [22]. This algorithm is resilient to noise and occlusions in the images of the recorded intensity patterns. Furthermore, sub-pixel precision is achieved by calculating a weighted centroid around the Fourier peak, eliminating the need for extensive upsampling of the Fourier transforms. In contrast, the first-order component of the Fourier Transform provides a deterministic assessment of ΔY as interferences typically exhibit a single frequency. This approach has been previously employed for phase extraction from interferograms [23].

The image registration algorithm uses the Fourier shift theorem [22], which relates shifts in real space to phase differences in the frequency domain. By taking the inverse Fourier Transform of the cross-power spectrum, derived from the 2D Fourier Transform of the interferogram images, the position of the peak corresponding to the fringe shift (ΔY) is determined. The reliability of these values depend on the signal response of the cross-power spectrum, which is normalized to unity. The closer this response is to one, the more dependable the algorithm's results are, indicating a distinct peak that accurately reflects the image shift.

The lateral fringe shift is $\Delta Y = \Delta\phi(L/2\pi)$, where $\Delta\phi$ and L are the relative phase and the period of the interferogram, respectively. From the double-slit geometry, L can be written as $L = \lambda s/d$ where s is the slit-to-detector distance, and d is the separation between the two slits. Substituting the relative phase in terms of the path length difference $\Delta\phi = -k\delta(\omega)t_f$, we can combine these expressions to rewrite the lateral fringe shift as

$$\Delta Y_\sigma = \frac{(\delta_\sigma(\omega) - \delta_{\sigma o}(\omega))st_f}{d}, \tag{1}$$

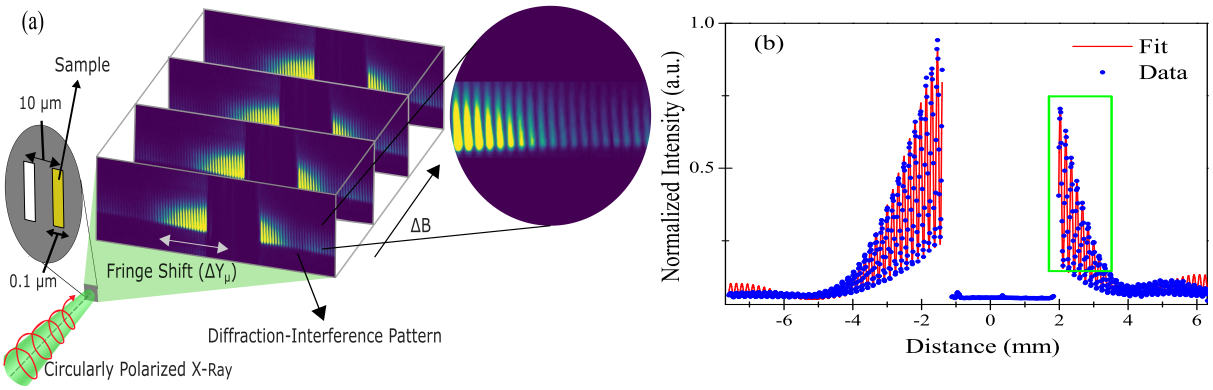

FIG. 1. (a) Schematic diagram of the soft x-ray Young's Double slit experimental set-up, with images recorded as a function of external OOP field at the Fe L_3 edge (707 eV). A zoomed-in view of the CCD images showcases the interference-diffraction pattern. (b) The resulting normalized intensity data (blue circles) overlapped with the resulting normalized intensity expression (red line) obtained from a non-linear least squares fit to the data. The missing intensity data at the center is due to the beamstop blocking part of the beam. The green rectangle highlights the intensity line cut region utilized in the analysis of the supplementary video files which show fringe movement with changing magnetic field. The period recording one fringe was found to be approximately 12 pixels which is equivalent to 162 μm, consistent with the double slit fringe width or spatial period estimate of w_f =162.66 μm. Details of this calculation can be found in the supplementary file.

where $\delta_{\sigma o}$ represents the zero field fringe shift pattern of the interferogram for $\sigma = \pm$ polarized light, which has an inherent phase accumulation due to the thickness of the film covering one of the slits. The complex component of the refractive index $\beta(\omega)$ accounts for x-ray absorption, and has no affect on the lateral fringe shift.

Figure 1(b) shows normalized 1D line-cuts extracted from the CCD images. We observe high contrast fringes with an intensity envelope as expected from double slit diffraction. The data were fitted with an intensity expression.

$$I = I_o \frac{\sin^2 \alpha}{\alpha^2} \cosh \tilde{\beta} \left(\frac{\sin \theta}{\theta} \cos \tilde{\gamma} + \cosh \tilde{\beta} \right) \qquad (2)$$

where $\tilde{\beta} = k\beta t_f$ and $\tilde{\gamma} = 2\gamma - k\delta t_f$. The above equation was derived using the concepts of Fraunhofer diffraction [24]. A detailed derivation of this equation can be found in the supplementary material. In this expression $\alpha = kby/2s$, where y is the vertical position on the detector and b is the slit width; $\gamma = kdy/2s$, where d is the slit separation. The parameter θ controls the envelope function $\frac{\sin\theta}{\theta}$ which represents the beam's coherence and affects fringe visibility [25]. Keeping the parameters k, s and t_f constant, we perform a non-linear least squares fitting of the intensity pattern. Further details explaining the use of the fitting algorithm (to extract β) and the shift registration algorithm (to extract δ) can be found in the supplementary file. Fig. 1(b) shows how the fitted expression compares to the normalized intensity data points. From the initial fits, we determine the dimensions of the double slit grating such as the slit width b and slit separation d to be 101.17 nm and 10.12 μm respectively, which is consistent with the nominal values of 100 nm and 10 μm. Successfully verifying these slit parameters reinforces the reliability of the intensity data and the fitting expression.

In Fig. 2(a), we show the hysteresis loop in the phase shift due to the field-induced phase change of the signal. Figure 2(a) shows the hysteresis curves from the fringe shift for the σ_+ (ΔY_+) and σ_- (ΔY_-) beams, denoted by the blue and red curves, respectively. A striking difference is evident in the directionality of the fringe shifts between the ΔY_+ and ΔY_- curves. Both the curves exhibit a familiar hysteresis behavior, with the fringes shifting in opposite directions under similar field conditions, though to varying degrees.

Figure 2(b) is the loop obtained by subtracting the two separate loops ($\Delta Y_+ - \Delta Y_-$) giving us a signal proportional to the net magnetization. We overlay the data with smoothed curves, shown as dotted lines, generated using a Savitzky-Golay filter to highlight the overall trajectory of the fringe pattern [26]. Applying Eq. (1) we can say that for $\Delta Y \sim 0.1$ μm, the corresponding magnetically induced changes in $\Delta\delta(\omega) \sim 5 \times 10^{-5}$. The difference $\Delta Y_+ - \Delta Y_-$ stabilizes at 1.5 μm.

The expression for dispersion in the x-ray regime is given by $\delta(\omega) = n_a r_e \lambda^2 f_1^0/2\pi$ where n_a is the atomic number density of the species and r_e is the electron radius [1]. This expression, in conjunction with Eq. (1), enables us to relate the fringe shift change to the number of electrons that produces the refraction index change. The recorded fringe shifts in micrometers are scaled to

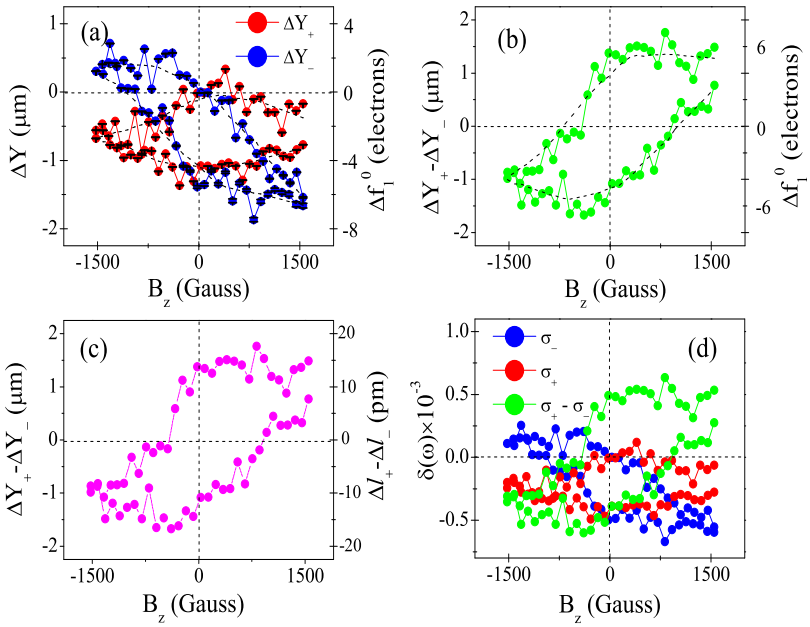

FIG. 2. Experimental fringe shift recorded through the magnetic hysteresis. (a) shows the registered fringe displacement for circularly polarized light. The error bars are smaller than the data points (visible upon magnifying the image). Data in the subsequent panels are derived from (a). Error bars are not displayed. (b) shows the difference between the two curves. The axis on the right-hand side shows the corresponding change in the scattering factor values (Δf_1^0). (c) Shows the difference between the two curves scaled to the difference in the magnetic path length. (d) Shows the hysteresis curves for σ_+, σ_- and $\sigma_+ - \sigma_-$ light scaled to display the changes in their respective $\delta(\omega)$ values with respect to their δ values at $B_z = 0$ Gauss.

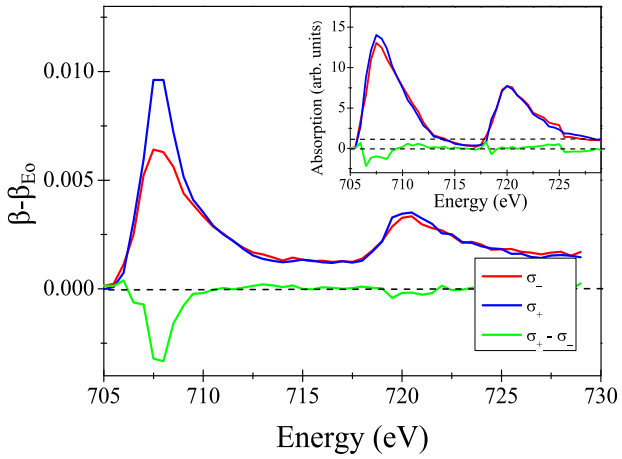

FIG. 3. The complex part of the refractive index vs Energy obtained from the fitting of the interferogram. Inset showcases the diode current values normalized as a measure of XMCD absorption. The red, blue, and green curves correspond to σ_- light, σ_+ light, and the dichroic signal ($\sigma_+ - \sigma_-$), respectively.

$\delta(\omega) - \delta_o(\omega)$ using Eq. (1) by substituting the known values of the Fe/Gd thickness t_f, detector-sample separation s, and slit separation d. Incorporating the previously mentioned expression for the x-ray dispersion, $\delta(\omega) - \delta_o(\omega)$ is scaled to represent the change in the number of electrons contributing to the magnetic moment $f_1^0(\sigma, \mathbf{B}) - f_1^0(\sigma, 0) = \Delta f_1^0(\sigma)$. The atomic number density of the Fe/Gd sample is estimated by calculating the stoichiometric weighted mean of the elemental number densities using the expression $n_a = N_A \rho / M$ where ρ is the mass density of the element, M is the molar mass and N_A is Avogadro's number This calculation yields an atomic number density of 8.53×10^{28} atoms/m^3 enabling us to retrieve Δf_1^0 from the fringe shift data. Furthermore, to plot the change in the magnetic path length l_m as shown in Fig. 2(c) we employ the expression $l_m = (1 - \delta(\mathbf{m}))t_f$ resulting in a direct relation between the relative path length difference and the relative change in the dispersion $\Delta l_m = -\Delta\delta t_f$. In Fig. 2(d), we show the relative change in the δ values (the real part of the refractive index) for σ_+ and σ_- light, along with their difference, as determined from the measured fringe shifts. The plots reveal that the difference $\delta(\sigma_+) - \delta(\sigma_-)$ stabilizes at approximately 5×10^{-4}. Note, the order of magnitude of the extracted $\delta(\omega)$ values are consistent with those reported in the literature [27]. Although we are in the ballpark, our value is still lower than the one quoted by Kortright. Our sample is FeGd, which is not fully saturated, while Kortright used elemental Fe. This

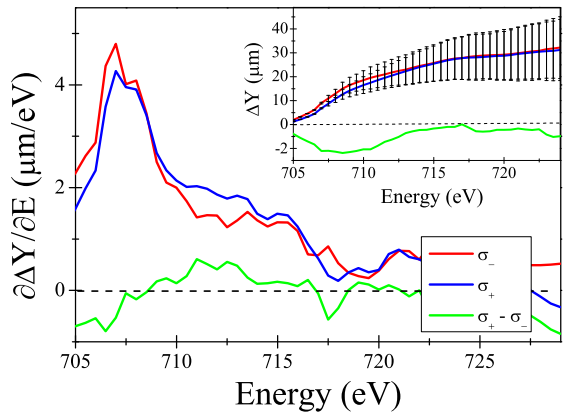

FIG. 4. The rate of fringe shift as a function of the photon energy as measured by the image registration algorithm. The inset tracks the absolute shift for σ_+ and σ_-. The difference between $\sigma_+ - \sigma_-$ is scaled by a factor of five to enhance its visibility. The red, blue, and green curves correspond to σ_- light, σ_+ light, and the dichroic signal ($\sigma_+ - \sigma_-$), respectively.

could possibly explain the discrepancy between the two values.

To illustrate the capability of the double slit to isolate the Fe L_3 edge at approximately 707 eV, we performed energy scans and extracted the $\beta(\omega)$ parameter from the resulting interferograms using the method described earlier, shown in Fig. 3. The energy scans were carried out from 705 eV to 730 eV at $B = 0$ Gauss. The β fit values were subtracted by β_{Eo}, which is the β value at zero field for the first energy value in the scan (705 eV), to track the relative change in the β parameter. The two sharp peaks correspond to the Fe absorption edges and exhibit the XMCD effect, appearing as a differential absorption between the two helical beams. The peaks in the $\beta(\omega)$ fits are consistent with the peaks seen in the absorption data (shown in Fig. 3 inset). The diode current used to measure the absorption is contributed only by the slit over the sample's surface. The beginning and starting of the energy ranges were normalized to lie between 0 and 1 to represent the ionization from the $2p$ level. The peaks at the L_3 and L_3 edges represent the electrons undergoing the $2p \longrightarrow 3d$ transition. We note that the differential absorption is pronounced at the L_3 edge, but this is not the case at the L_2 edge. A similar lack of absorption contrast has previously been observed in $Fe_3Gd_3O_{12}$, where Gd atoms are antiferromagnetically coupled to the Fe moments, reducing the net magnetization at the L_2 energy [28].

In Fig. 4, we demonstrate the spectroscopic capability of the double slit set-up. We show that it is possible to isolate the Fe L_3 edge by tracking how the fringe positions change with the increasing photon energy for σ_+ and σ_- light. The inset shows the absolute fringe shift determined using the shift registration algorithm previously described in the context of Fig. 2. By computing the derivative of the fringe shift with respect to the photon energy, we obtain a dominant peak as illustrated in the main panel, which plots $\partial\Delta Y/\partial E$ vs E. Using this approach, we are able to reproduce the features of Fig. 3, particularly the dominant peak at 707 eV, which corresponds to the L_3 edge. While this was not the primary objective of the study, this illustrates that the double-slit setup can also serve as a spectroscopic tool. The fringes move rapidly because of the steep changes in the refractive index near this edge. The magnetic sensitivity is also enhanced at these energy ranges. However, dramatic fluctuations in the intensity pattern across the energy spectrum can compromise the accuracy of the image registration algorithm. This limitation may account for the difficulty in detecting more subtle features, such as the Fe L_2 edge, via fringe shifts in the energy scans.

The sensitivity of the set-up is determined by the smallest detectable change in the dispersive part of the refractive index $\delta(\omega)$, derived from the quantitative measurement of the fringe shift ΔY. A conservative estimate of the registration algorithm allows for a minimum reliable detectable shift ΔY_{min} of 0.01 pixels [22]. Plugging this into a rearranged iteration of Eq (1) yields $\Delta\delta_{min}(\omega) = \Delta Y_{min}(s_{pixel}/s)(d/t_f)$. This implies that the pixel size or resolution of the CCD detector along with the slit-to-detector distance s significantly impacts the sensitivity of the measurement. The separation between the two slits d is constrained by the focus precision of the milling ion beam. Essentially, the number of pixels per fringe peak, which corresponds to the image resolution of a single fringe, determines the accuracy with which $\Delta\delta(\omega)$ can be isolated. Experimental adjustments, such as extending s from 1 m to 5 m, combined with enhanced resolution, can improve the sensitivity of $\Delta\delta(\omega)$ to the order of 10^{-6}.

In conclusion, we have presented an innovative and straightforward approach for accurately measuring the dispersion of a Fe/Gd film using a modified Young's double-slit setup. This was demonstrated at the Fe L_3 edge using the contrast between circularly polarized light to obtain the net magnetic contribution to the dispersion changes. The results are applicable to any coherent light source and can be further enhanced with alternative reconstruction schemes to improve precision. Further experiments and studies can entail modifications such as increasing the detector-sample separation to allow the registration of even smaller changes, increasing the sensitivity. Using a revised double-slit setup, where only the top half of one slit is covered by the thin film, can generate two stacked interferograms, providing a reference

fringe pattern to more accurately track the fringe shifts. Our work also opens the door to exploring quantum materials like ferroelectrics and multiferroics, where optical properties change under an applied electric field. Additionally, combining single-shot differential measurements from the double-slit setup with a pump-probe experiment and time-resolved spectroscopy could offer an avenue to investigate Floquet physics in quantum materials by capturing time-dependent changes in the refractive index.

The authors thank Prof. Eric. E. Fullerton of UC San Diego for important discussions and insight. T.D. thanks Tom Colbert for insightful discussions on optics. This work was supported in part by the US Department of Energy Office of Science, Office of Workforce Development for Teachers and Scientists (WDTS) under the Science Undergraduate Laboratory Internship (SULI) program. Work at the ALS, LBNL was supported by the Director, Office of Science, Office of Basic Energy Sciences, of the US DOE (Contract No. DE-AC02-05CH11231)

[1] J. Als-Nielsen and D. McMorrow, *Elements of Modern X-ray Physics* (John Wiley & Sons, Ltd, 2011, The Atrium, Southern Gate, Chichester, West Sussex, PO19 8SQ, United Kingdom, 2011).

[2] J. Stöhr and H. C. Siegmann, *Magnetism: From Fundamentals to Nanoscale Dynamics* (Springer Science & Business Media, 2007, London, 2007).

[3] P. Norman and A. Dreuw, Simulating x-ray spectroscopies and calculating core-excited states of molecules, *Chemical Reviews*, Chemical Reviews **118**, 7208 (2018).

[4] A. Sakdinawat and D. Attwood, Nanoscale x-ray imaging, Nature Photonics **4**, 840 (2010).

[5] C. Sanchez-Cano, R. A. Alvarez-Puebla, J. M. Abendroth, T. Beck, R. Blick, Y. Cao, F. Caruso, I. Chakraborty, H. N. Chapman, C. Chen, B. E. Cohen, A. L. C. Conceição, D. P. Cormode, D. Cui, K. A. Dawson, G. Falkenberg, C. Fan, N. Feliu, M. Gao, E. Gargioni, C.-C. Glüer, F. Grüner, M. Hassan, Y. Hu, Y. Huang, S. Huber, N. Huse, Y. Kang, A. Khademhosseini, T. F. Keller, C. Körnig, N. A. Kotov, D. Koziej, X.-J. Liang, B. Liu, S. Liu, Y. Liu, Z. Liu, L. M. Liz-Marzán, X. Ma, A. Machicote, W. Maison, A. P. Mancuso, S. Megahed, B. Nickel, F. Otto, C. Palencia, S. Pascarelli, A. Pearson, O. Peñate-Medina, B. Qi, J. Rädler, J. J. Richardson, A. Rosenhahn, K. Rothkamm, M. Rübhausen, M. K. Sanyal, R. E. Schaak, H.-P. Schlemmer, M. Schmidt, O. Schmutzler, T. Schotten, F. Schulz, A. K. Sood, K. M. Spiers, T. Staufer, D. M. Stemer, A. Stierle, X. Sun, G. Tsakanova, P. S. Weiss, H. Weller, F. Westermeier, M. Xu, H. Yan, Y. Zeng, Y. Zhao, Y. Zhao, D. Zhu, Y. Zhu, and W. J. Parak, X-ray-based techniques to study the nano–bio interface, ACS Nano **15**, 3754 (2021), pMID: 33650433, https://doi.org/10.1021/acsnano.0c09563.

[6] Q. Saadeh, V. Philipsen, J. Meersschaut, V. S. K. Channam, K.-A. Kantre, A. Sokolov, B. Kupper, T. Wiesner, D. O. na García, Z. Salami, C. Buchholz, F. Scholze, and V. Soltwisch, Optical constants of tin, amorphous sio2, and sin in the extreme ultraviolet range, Appl. Opt. **63**, 9210 (2024).

[7] J. Kas, F. Vila, C. Pemmaraju, M. Prange, K. Persson, R. Yang, and J. Rehr, Full spectrum optical constant interface to the materials project, Computational Materials Science **201**, 110904 (2022).

[8] V. Lucarini, J. Saarinen, K. Peiponen, and E. Vartiainen, Kramers-kronig relations in optical materials research, Kramers-Kronig Relations in Optical Materials Research, by V. Lucarini, J. Saarinen, K. Peiponen, and E. Vartiainen. X, 162 p. 37 illus. 3-540-23673-2. Berlin: Springer, 2005. **110** (2005).

[9] M. Blume and D. Gibbs, Polarization dependence of magnetic x-ray scattering, Phys. Rev. B **37**, 1779 (1988).

[10] J. P. Hill and D. F. McMorrow, Resonant Exchange Scattering: Polarization Dependence and Correlation Function, Acta Crystallographica Section A **52**, 236 (1996).

[11] B. T. Thole, P. Carra, F. Sette, and G. van der Laan, X-ray circular dichroism as a probe of orbital magnetization, Phys. Rev. Lett. **68**, 1943 (1992).

[12] C. Kao, J. B. Hastings, E. D. Johnson, D. P. Siddons, G. C. Smith, and G. A. Prinz, Magnetic-resonance exchange scattering at the iron l_{ii} and l_{iii} edges, Phys. Rev. Lett. **65**, 373 (1990).

[13] A. Scherz, W. F. Schlotter, K. Chen, R. Rick, J. Stöhr, J. Lüning, I. McNulty, C. Günther, F. Radu, W. Eberhardt, O. Hellwig, and S. Eisebitt, Phase imaging of magnetic nanostructures using resonant soft x-ray holography, Phys. Rev. B **76**, 214410 (2007).

[14] S. Eisebitt, M. Lörgen, W. Eberhardt, J. Lüning, J. Stöhr, C. T. Rettner, O. Hellwig, E. E. Fullerton, and G. Denbeaux, Polarization effects in coherent scattering from magnetic specimen: Implications for x-ray holography, lensless imaging, and correlation spectroscopy, Phys. Rev. B **68**, 104419 (2003).

[15] J. Neethirajan, B. J. Daurer, M. D. P. Martínez, A. c. v. Hrabec, L. Turnbull, R. Yamamoto, M. R. Ferreira, A. c. v. Štefančič, D. A. Mayoh, G. Balakrishnan, Z. Pei, P. Xue, L. Chang, E. Ringe, R. Harrison, S. Valencia, M. Kazemian, B. Kaulich, and C. Donnelly, Soft x-ray phase nanomicroscopy of micrometer-thick magnets, Phys. Rev. X **14** (2024).

[16] Ph.D. thesis.

[17] P. Carra, B. T. Thole, M. Altarelli, and X. Wang, X-ray circular dichroism and local magnetic fields, Phys. Rev. Lett. **70**, 694 (1993).

[18] C. Chang, E. Anderson, P. Naulleau, E. Gullikson, K. Goldberg, and D. Attwood, Direct measurement of

index of refraction in the extreme-ultraviolet wavelength region with a novel interferometer, Opt. Lett. **27**, 1028 (2002).

[19] J. W. Freeland, K. Bussmann, Y. U. Idzerda, and C.-C. Kao, Understanding correlations between chemical and magnetic interfacial roughness, Phys. Rev. B **60**, R9923 (1999).

[20] S. Roy, M. R. Fitzsimmons, S. Park, M. Dorn, O. Petracic, I. V. Roshchin, Z.-P. Li, X. Batlle, R. Morales, A. Misra, X. Zhang, K. Chesnel, J. B. Kortright, S. K. Sinha, and I. K. Schuller, Depth profile of uncompensated spins in an exchange bias system, Phys. Rev. Lett. **95**, 047201 (2005).

[21] J. C. T. Lee, J. J. Chess, S. A. Montoya, X. Shi, N. Tamura, S. K. Mishra, P. Fischer, B. J. McMorran, S. K. Sinha, E. E. Fullerton, S. D. Kevan, and S. Roy, Synthesizing skyrmion bound pairs in Fe-Gd thin films, Applied Physics Letters **109**, 022402 (2016).

[22] H. Foroosh, J. Zerubia, and M. Berthod, Extension of phase correlation to subpixel registration, IEEE Transactions on Image Processing **11**, 188 (2002).

[23] K. A. Goldberg and J. Bokor, Fourier-transform method of phase-shift determination, Appl. Opt. **40**, 2886 (2001).

[24] M. Born, E. Wolf, A. B. Bhatia, P. C. Clemmow, D. Gabor, A. R. Stokes, A. M. Taylor, P. A. Wayman, and W. L. Wilcock, *Principles of Optics: Electromagnetic Theory of Propagation, Interference and Diffraction of Light*, 7th ed. (Cambridge University Press, 1999).

[25] D. P. Jackson, N. Ferris, R. Strauss, H. Li, and B. J. Pearson, Subtleties with Young's double-slit experiment: Investigation of spatial coherence and fringe visibility, American Journal of Physics **86**, 683 (2018).

[26] A. Savitzky and M. J. E. Golay, Smoothing and differentiation of data by simplified least squares procedures., Analytical Chemistry **36**, 1627 (1964).

[27] J. B. Kortright and S.-K. Kim, Resonant magneto-optical properties of fe near its 2p levels: Measurement and applications, Phys. Rev. B **62**, 12216 (2000).

[28] P. Rudolf, F. Sette, L. Tjeng, G. Meigs, and C. Chen, Magnetic moments in a gadolinium iron garnet studied by soft-x-ray magnetic circular dichroism, Journal of Magnetism and Magnetic Materials **109**, 109 (1992).